Medium modification of photon-tagged jets at the LHC

Guang-You Qin

Department of Physics, Duke University, Durham, North Carolina 27708, USA
(Dated: October 25, 2012)

We study the medium modification of jets correlated with large transverse momentum photons at the LHC via a Monte-Carlo transport model which incorporates both elastic collisions and radiative energy loss experienced by the parton showers. Numerical results are presented for the modification of tagged jet yield, the photon-jet momentum imbalance, and their azimuth separation distribution. The use of photon-jet correlations as jet quenching tomography tools is addressed by studying the photon-jet events with different values of $x_T = p_{T,J}/p_{T,\gamma}$. It is found that larger x_T jets are mainly produced from the surface of the medium, while smaller x_T jets are from those jets which have traversed longer distance of medium. Combined with the momentum spectrum of the photon-tagged jets, this leads to stronger suppression and centrality dependence for larger x_T jets, and weaker suppression (or enhancement) for smaller x_T jets.

The energetic probes produced in early hard scattering processes provide valuable tools for studying the properties of the quark-gluon plasma (QGP) created in relativistic heavy-ion collisions. Large transverse momentum (p_T) jets are particularly useful as they directly interact with the constituents of the dense QCD matter that they traversed, and are modified/quenched in the process [1]. Jet quenching has been confirmed by multiple experimental observations, such as the significant suppression of single inclusive high p_T hadron production in nucleus-nucleus collisions compared to binary collision scaled proton-proton collisions at the same energies [2–4].

A lot of effort has been devoted to understand the modification of jets by the hot and dense strongly-interacting QCD matter. Jet modification originates from a combination of drag, diffusion and stimulated gluon emission experienced by the partonic jets while propagating through the highly excited nuclear medium [5–8]. Various transport coefficients, e.g., $\hat{e} = dE/dt$, $\hat{e}_2 = d(\Delta E)^2/dt$ and $\hat{q} = d(\Delta p_T)^2/dt$, have been employed to quantify these modification effects [8, 9]. There are currently a number of perturbative QCD based schemes for the treatment of the radiative part of parton energy loss [10–14]. A systematic comparison of these different jet quenching schemes has been carried out in Ref. [15] in terms of the "brick" problem. Many phenomenological calculations have been performed to describe the observed jet modification measurements, such as the suppression of single inclusive high p_T hadron production [16–20], and the nuclear modification of dihadron [21, 22] and photon-hadron [23–25] correlations in high energy nucleus-nucleus collisions.

Recently, sophisticated experimental techniques have been developed to reconstruct the full jets emitted in relativistic heavy-ion collisions. This provides more stringent test on our understanding of jet modification in terms of both leading and subleading fragments of the jet showers

[26]. Various Monte-Carlo generators are being developed to simulate the modification of jet propagation in dense nuclear medium [27–30]. The study of in-medium evolution of the full jets helps to understand how energy and momentum are deposited by the jet showers and how the medium responds to jet propagation and energy deposition [31–33].

Meanwhile, the much larger kinematics achieved at the LHC now allows us to investigate medium effects on jets with very large transverse energies (over a hundred GeV). One of the first exciting full jet results from the LHC is the strong modification of the momentum imbalance distribution between the correlated jet pairs in central Pb+Pb collisions, while no strong modification is observed for the dijet relative azimuth separation distribution [34, 35]. This result indicates significant energy loss experienced by the subleading jets during their propagating through the hot and dense medium created in Pb+Pb collisions. There have been various models employed to explain the observed dijets asymmetry in Pb+Pb collisions at the LHC [36–42].

Another promising observable is the modification of the jets correlated with photons or electroweak bosons in relativistic heavy-ion collisions. Such channel has been regarded as the "golden" channel for jet quenching study due to the fact that the neutral boson triggers, once produced, will escape the medium without further interaction. Thus a stronger constraint is provided by the triggers for the away-side tagged jets that we are interested in [43]. Furthermore, many biases that are present in single inclusive jet/hadron suppression and dijet/dihadron/jet-hadron correlations are improved, such as the deep falling spectra, trigger bias, and the sensitivity to the background fluctuations. Experimental measurements of photon-triggered fragmentation function at RHIC [44, 45] and the momentum imbalance of correlated photon-jet pairs at the LHC [46] are consis-

tent with parton energy loss calculations [23–25, 47, 48].

In this work, we focus on studying the medium modification of jets correlated with high p_T photons at the LHC energies. A Monte-Carlo transport code is developed to simulate in-medium jet shower evolution and jet modification in dense QCD medium, with the inclusion of both stimulated gluon radiation and the elastic collisions experienced by the shower partons. The effect of elastic collisions is quantified by a few transport coefficients, namely the longitudinal drag and diffusion as well as transverse momentum broadening, while the radiative energy loss is simulated by employing the single gluon emission spectrum obtained from Higher Twist jet energy loss calculation [13, 14]. In section II, we provide some details of how the simulation of jet shower transport in medium is performed. The numerical results for photon-jet correlations in Pb+Pb collisions at the LHC energies are presented in section III, where we address the use of photon-jet correlations as jet quenching tomography tools by studying the tagged jets with different x_T values. The last section contains our summary.

I. IN-MEDIUM JET TRANSPORT

In this section, we describe our Monte-Carlo method for simulating the transport and modification of a partonic jet shower in dense QCD matter. We assume each parton of the jet shower follows classical trajectories between each jet-medium interaction that induces the momentum change of the parton (either by an elastic collision or the radiation of a gluon). We keep track of all the propagating partons and the radiative gluons until they traverse the dense medium.

The probability for a parton at each time step Δt to have an momentum exchange by an elastic collision with the medium constituents is determined by,

$$P_{\text{coll}}(t, \Delta t) = \Delta t / t_{\text{mf}} \qquad (1)$$

where t_{mf} is an "effective" mean free time, thus $1/t_{\text{mf}}$ is the rate of the elastic collisions (energy and momentum exchange). If there is a jet-medium interaction through an elastic collision, the energy and momentum exchange is sampled from a probability distribution of $P(\Delta E, \Delta \vec{p}_\perp, t, \Delta t)$.

Generally, the above mean free time t_{mf} and the distribution of the momentum and energy exchange can be determined if the details about the medium structure and jet-medium interaction are known. In this application, we assume that the probability distribution $P(\Delta E, \Delta \vec{p}_\perp, t, \Delta t)$ is a Gaussian distribution in both longitudinal and transverse directions, with the mean and invariance provided by the longitudinal drag $\hat{e} t_{\text{mf}}$ and diffusion $\hat{e}_2 t_{\text{mf}}$, and transverse broadening $\hat{q} t_{\text{mf}}$.

The Gaussian form for the momentum exchange through the elastic collisions originates from the assumption of multiple scatterings with small momentum transfer for each scattering. Such limit corresponds to setting

the mean free time equal to the time step ($t_{\text{mf}} = \Delta t$), i.e., the Langevin approach. The variation of t_{mf} values does not affect the results for Gaussian form of momentum exchange and large extent of the medium ($\Delta t \leq t_{\text{mf}} \ll L$). Realistic values of mean free time t_{mf} may be used in the future study when the method is extended to include the case when the momentum exchange is a non-Gaussian form, such as few hard collisions with a power-law tail.

We simulate the radiation of gluons by employing the single gluon emission spectrum from the higher twist calculation [13, 14],

$$\frac{dN_g}{dx dl_\perp^2 dt} = \frac{2\alpha_s}{\pi} P(x) \frac{\hat{q}}{l_\perp^4} \sin^2\left(\frac{t - t_i}{2 t_{\text{form}}}\right) \qquad (2)$$

where x and $l_\perp$ are the fractional energy and transverse momentum carried by the radiated gluon. $P(x)$ is the vacuum splitting function, and $t_{\text{form}} = 2Ex(1-x)/l_\perp^2$ is the gluon formation time.

The probability for a parton in each time step Δt to radiate a gluon is determined by the average number of gluons:

$$P_{\text{rad}}(t, \Delta t) = \langle N_g(t, \Delta t) \rangle = \Delta t \int dx dl_\perp^2 \frac{dN_g}{dx dl_\perp^2 dt} \qquad (3)$$

If there is a gluon emitted in a given time step, the energy and the momentum of the radiated gluon are sampled from the following probability distribution,

$$P(x, l_\perp^2, t, \Delta t) = \frac{\Delta t}{\langle N_g \rangle} \frac{dN_g}{dx dl_\perp^2 dt} \qquad (4)$$

To simulate the medium modification of jet shower, we need to provide the initial conditions before the jet-medium interaction. In this application, the production of the photon-jet pairs from early hard scattering processes are generated from PYTHIA8.1 [49] for p+p collisions at $\sqrt{s_{NN}} = 2.76$TeV. The full jet reconstruction is performed via FASTJET package [50] from which one can find the detailed content of the full jets, such as the energy and momentum for each parton in a jet. Such initial conditions are provided to our Monte-Carlo code for the further simulation of in-medium transport and medium modification.

The initial photon-jet production points is sampled according to the distribution of the binary collisions simulated from the Glauber Model. The evolution profiles (energy/entropy density, temperature and flow velocities) of the bulk QGP medium that jets interact with is provided by hydrodynamic simulation. In this work, we employ the (2+1)D viscous hydrodynamics model (VISH2+1) developed by The Ohio State University group [51–53], with two-component Glauber model for hydrodynamics initial conditions. The code version and parameter tunings for Pb+Pb collisions at LHC energies are taken as in Ref. [53].

When simulating the propagation of the jet shower through the hydrodynamic medium, we only allow the vacuum radiated gluons to interact with the medium

when their formation times t_{form} are reached. We impose a minimum energy cutoff πT for the medium-induced radiation spectrum in order to take into account the balance between gluon radiation and absorption from the hydrodynamic medium. When the local temperature of the medium drops below the transition temperature 160MeV, jets are assumed to decouple from the medium. After jets traverse the hydrodynamic medium, we provide the detailed information of the modified jets to FAST-JET package to perform the jet reconstruction and then compare with the vacuum jets. In this work, we have not included the hadronization process which we postpone to an upcoming effort.

As mentioned above, the jet shower evolution in dense QGP medium are controlled by three transport coefficients $\hat{e}$, $\hat{e}_2$ and $\hat{q}$. Thse coefficients can be calculated if the detailed information about medium structure and jet-medium interaction is known [54]. Here we assume that the diffusions in transverse and longitudinal directions are symmetric, and the fluctuation-dissipation relation may be applied between the drag and diffusion, $\hat{q} \approx 2\hat{e}_2 \approx 4T\hat{e}$. The functional form of the transport coefficients is taken as $\hat{q} \propto T^3$, with the overall normalization to be fitted to one data point. The sensitivity of jet in-medium transport and modification to different parameterizations of jet transport coefficients will be investigated in the future study.

II. NUMERICAL RESULTS FOR PHOTON-JET CORRELATIONS

In this section, we present some numerical results for the medium modification of jets correlated with high p_T photons in Pb+Pb collisions at $\sqrt{s_{NN}} = 2.76$TeV at the LHC. One of the most interesting quantities is the distribution of the tagged jet momentum fraction $x_T = p_{T,J}/p_{T,\gamma}$, which may be defined as

$$
\begin{aligned}
f(x_T) &= (1/N_\gamma)dN_{J\gamma}/dx_T \\
P(x_T) &= (1/N_{J\gamma})dN_{J\gamma}/dx_T
\end{aligned}
\tag{5}
$$

The above two definitions differ only by the normalization. Given the kinematic cuts for the trigger photons and associated jets, the former distribution is normalized to the fraction of photons having the associated jet pair $R_{J\gamma}$ and the latter gives unity when integrating out the momentum fraction x_T. The nuclear modification factor I_{AA} for the tagged jet distribution is usually defined as

$$
I_{AA}(x_T) = f_{AA}(x_T)/f_{pp}(x_T)
\tag{6}
$$

In Fig. 1 we show the x_T-integrated nuclear modification factor $I_{AA} = R_{J\gamma}^{AA}/R_{J\gamma}^{pp}$ (left) and the average fractional momentum loss $\langle \Delta x_T \rangle = \langle x_T \rangle|_{pp} - \langle x_T \rangle|_{AA}$ (right) as a function of centrality (the participant number N_{part}). The data points shown here are obtained from CMS measurements of $R_{J\gamma}$ and $\langle x_T \rangle$ for Pb+Pb collisions and PYTHIA+HYDJET references [46]). In
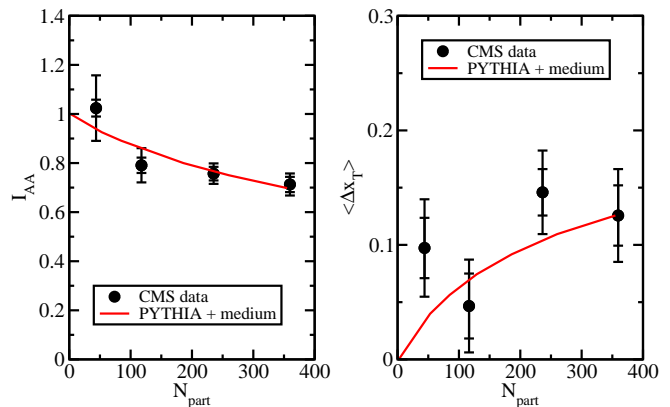

FIG. 1: (Color online) The nuclear modification factor I_{AA} and the average momentum loss $\langle \Delta x_T \rangle$ for photon-triggered jets as a function of centrality for Pb+Pb collisions at the LHC. The jet size is $R = 0.3$.

this work, the CMS kinematic cuts are taken for all the presented results: the photon momentum $p_{T,\gamma} > 60$GeV, jet momentum $p_{T,J} > 30$GeV, and their azimuth separation $\Delta\phi = |\phi_\gamma - \phi_J| < 7\pi/8$. The size of the jets is taken as $R = 0.3$ in this plot. The model parameter $\hat{q}$ (accordingly $\hat{e}$ and $\hat{e}_2$) is fitted to the value of $I_{AA} \approx 0.7$ in most central $(0-10\%)$ Pb+Pb collisions; we obtain the gluon transport coefficient $\hat{q}_0 = 6.5$GeV^2/fm at hydrodynamics initial time $\tau_0 = 0.6$fm/c. Due to stronger medium effect from peripheral to central collisions, one observes the decrease of the nuclear modification factor I_{AA} and the increase of the average fractional momentum loss $\langle \Delta x_T \rangle$ for the photon-triggered jets.
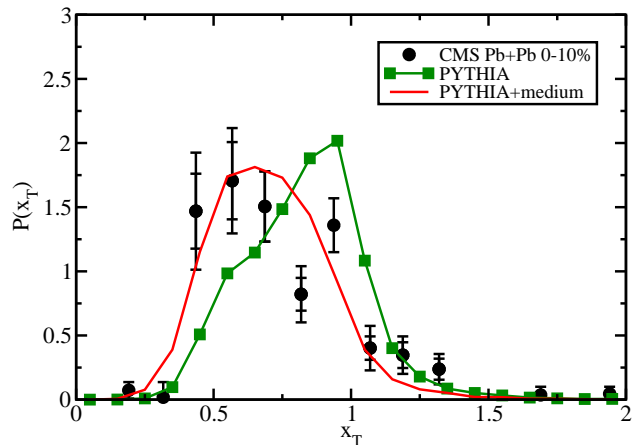

FIG. 2: (Color online) The distribution of the momentum imbalance variable x_T between triggered photons and associated jets for most central $(0-10\%)$ Pb+Pb collisions at the LHC. The jet size is $R = 0.3$.

One may look at the distributions of the momentum imbalance variable x_J between triggered photons and the away-side jets. In Fig. 2, the normalized distribution $P(x_T)$ is shown for both p+p and most central $(0-10\%)$
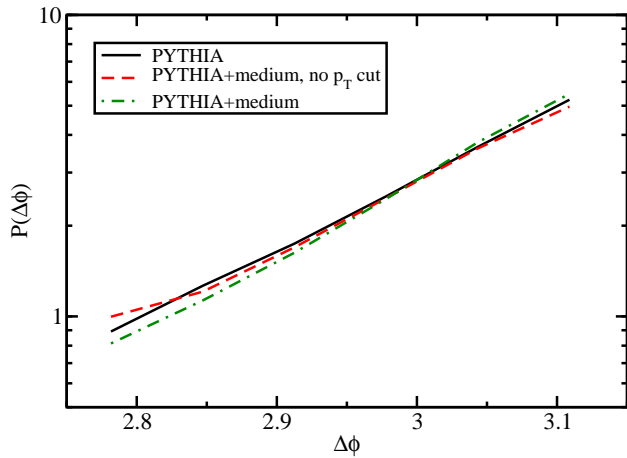
FIG. 3: (Color online) The distribution of the relative azimuth separation $\Delta\phi$ distribution between triggered photons and associated jets for most central $(0 - 10\%)$ Pb+Pb collisions at the LHC. The jet size is $R = 0.3$.

Pb+Pb collisions at the LHC. One observes the shift of the distribution to smaller x_J values for the distribution in Pb+Pb collisions compared to p+p collisions. This indicates that the tagged jets lose energy during its propagation through the hot and dense QGP created in the Pb+Pb collisions.

The azimuth separation between the trigger photons and associated jets $\Delta\phi = |\phi_\gamma - \phi_J|$ is another interesting quantity. In Fig. 3, the normalized distribution $P(\Delta\phi)$ is shown for both p+p collisions and most central $(0-10\%)$ Pb+Pb collisions. While there is strong modification for the momentum imbalance x_J distribution as shown in Fig. 2, no strong modification is observed for photon-jet azimuth separation $\Delta\phi$ distribution. This is partly due to the kinematic cuts applied on the selection of photon-jet events. Jets which are more strongly deflected by the dense medium are those having experienced larger energy loss. Thus after applying the kinematic cuts, many of such associated jets are not selected in the final result. Such effect is illustrated by the dashed curve which represents no p_T cut applied to the associated jet momentum after the in-medium evolution. One observes some broadening on the photon-jet azimuth separation $\Delta\phi$ distribution. Such broadening effect is further cut off by the constraint on the photon-jet azimuth separation $\Delta\phi > 7/8\pi$.

In Fig. 4 the photon-triggered nuclear modification factor I_{AA} is plotted as a function of the momentum fraction x_T for Pb+Pb collisions at the LHC. Results for different centralities are shown for comparison. One may observe that I_{AA} decreases from lower x_T values to higher x_T values. This means that the yield for the associated jets with high x_T values is suppressed in Pb+Pb collisions due to the interaction with the QGP medium, while the yield for lower x_T jets is enhanced due to the fact that the momentum fraction variable x_T distribution shifts from higher x_T to lower x_T values. We observe that
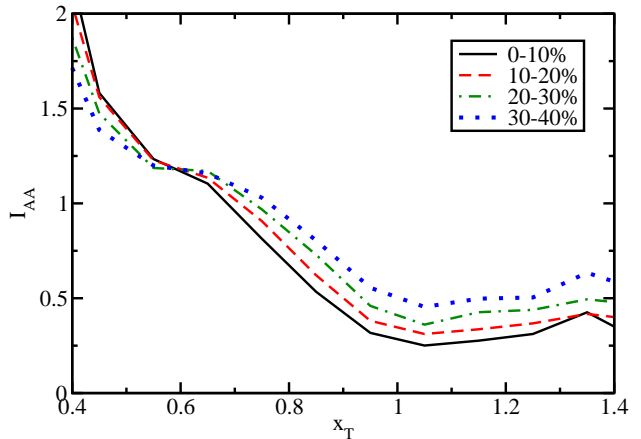

FIG. 4: (Color online) The nuclear modification factor I_{AA} for photon-triggered jets as a function of x_T for Pb+Pb collisions at the LHC in different centralities. The jet size is $R = 0.3$.
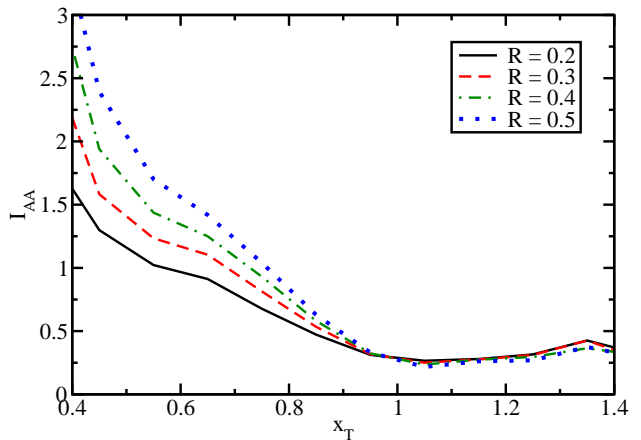

FIG. 5: (Color online) The nuclear modification factor I_{AA} for photon-triggered jets as a function of x_T for most central $(0 - 10\%)$ Pb+Pb collisions at the LHC. Results for different jet sizes are compared.

such medium modification effect increases from peripheral collisions to central collisions.

The above modification effect on the photon-triggered jets depends on the jet size. In Fig. 5 the photon-triggered nuclear modification factor I_{AA} is plotted as a function of x_T for most central $(0 - 10\%)$ Pb+Pb collisions at the LHC. Results for different jet sizes $(R = 0.2, 0.3, 0.4, 0.5)$ are shown for comparison. We observe that the suppression for the associated jet yield is similar for high x_T values for different jet sizes, and for smaller x_T values the enhancement is larger for larger jet size.

In the above, we have presented the medium modification of photon-triggered jet yield, the photon-jet momentum imbalance, and their azimuth separation distribution for Pb+Pb collisions at the LHC. Now we address the use of photon-triggered jets as a tomographic tool for studying jet quenching in relativistic heavy-ion collisions. In particular, we may classify the photon-jet
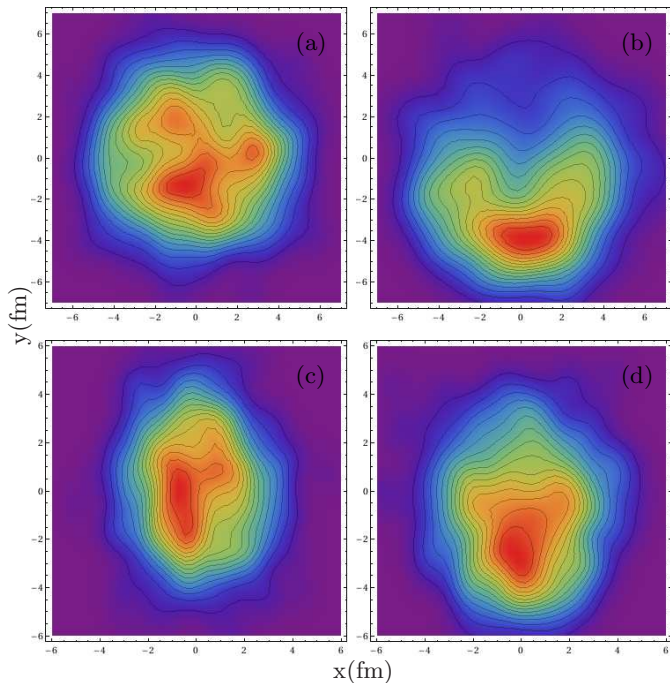
medium. Thus photon-triggered jets with different x_T values provide very useful tomographic tools for studying jet modification in relativistic heavy-ion collisions.
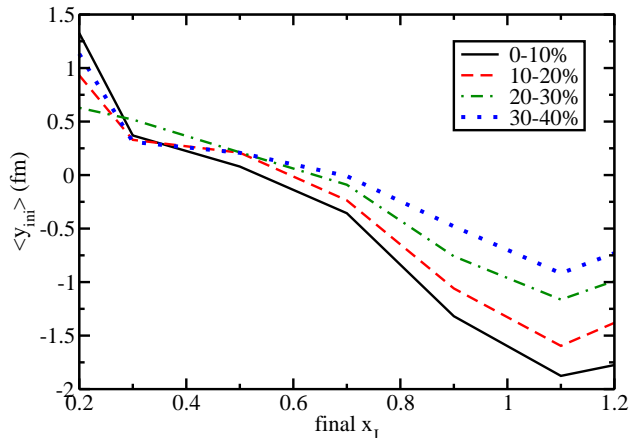

FIG. 6: (Color online) The density distribution of the initial photon-jet production points $(x_{\mathrm{ini}}, y_{\mathrm{ini}})$ when the triggered photons are taken along out-of-plane directions ($|\phi_\gamma - \pi/2| < \pi/12$) for Pb+Pb collisions at the LHC. Jets with different final x_T values are compared: $x_T = [0.5, 0.6]$ for (a) and (c); $x_T = [0.9, 1]$ for (b) and (d). Two different centralities are compared: $0 - 10\%$ for (a) and (b); $20 - 30\%$ for (c) and (d). The jet size is $R = 0.3$.

events according to different values of final x_T. This allows us to use photon-triggered jets to probe different regions of the hot and dense QGP created in the collisions. To illustrate this, we show in Fig. 6 the density distribution of initial photon-jet production points $(x_{\mathrm{ini}}, y_{\mathrm{ini}})$ in the transverse plane. Here we take those events with the triggered photons that propagate along out-of-plane directions ($|\phi_\gamma - \pi/2| < \pi/12$). We compare the initial photon-jet production point distribution for jets with different x_T values: $x_T = [0.5, 0.6]$ for (a) and (c); $x_T = [0.9, 1]$ for (b) and (d). Results for two different centralities are also shown for comparison: $0 - 10\%$ for (a) and (b); $20 - 30\%$ for (c) and (d). The jet size is taken as $R = 0.3$ in this plot.

If one takes photon-jet events for all values of x_T and propagating directions, the density distribution of initial photon-jet production points would follow binary collision distribution (if no kinematic cuts are applied after medium evolution). When selecting jet events with certain values of x_T, one can see that those jets with larger values of final x_T are mainly produced at the surface of the medium thus have traversed short medium length, while smaller x_T jets are more from these surviving jets which have traversed much longer distance. Combined with selecting trigger photons with different directions, we may probe different regions of the hot and dense

FIG. 7: (Color online) The average values of the jet initial production points $\langle y_{\mathrm{ini}} \rangle$ when the triggered photons are taken along out-of-plane directions ($|\phi_\gamma - \pi/2| < \pi/12$) for Pb+Pb collisions at the LHC. Results for different centralities are compared. The jet size is $R = 0.3$.
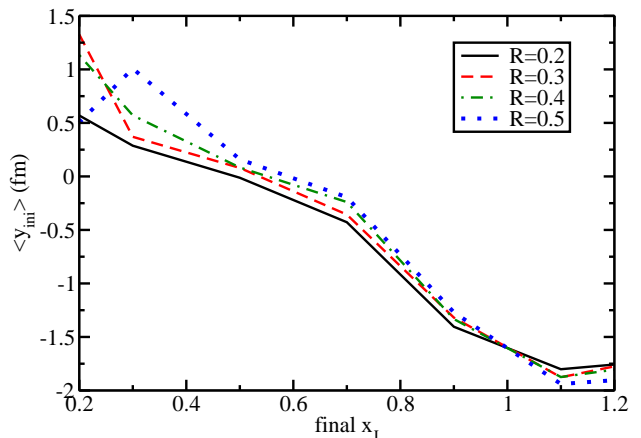

FIG. 8: (Color online) The average values of the jet initial production points $\langle y_{\mathrm{ini}} \rangle$ when the triggered photons are taken along out-of-plane directions ($|\phi_\gamma - \pi/2| < \pi/12$) for central $0 - 10\%$ Pb+Pb collisions at the LHC. Results for different jet sizes are compared.

The above effect can be made more quantitative. In Fig. 7, we show the average values for the photon-jet initial production points $\langle y_{\mathrm{ini}} \rangle$ if one looks at the triggered photons that propagate along out-of-plane directions ($|\phi_\gamma - \pi/2| < \pi/12$). One may see that on average jets with smaller x_T values may have traversed about a few fm longer distance than larger x_T jets. It is noted that such extra traveled path is the hottest part of the QGP medium. We observe that such effect is larger for central collisions than peripheral collisions.

The jet size dependence of the above effect is shown

in Fig. 8, where the average values of the jet initial production points $\langle y_{\text{ini}} \rangle$ is plotted as a function of x_T for most central $(0 - 10\%)$ Pb+Pb collisions at the LHC. The triggered photons is taken to be along out-of-plane directions $(|\phi_\gamma - \pi/2| < \pi/12)$ as above. One observes that the above effect show weak dependence on the jet size (stronger for larger jet size).
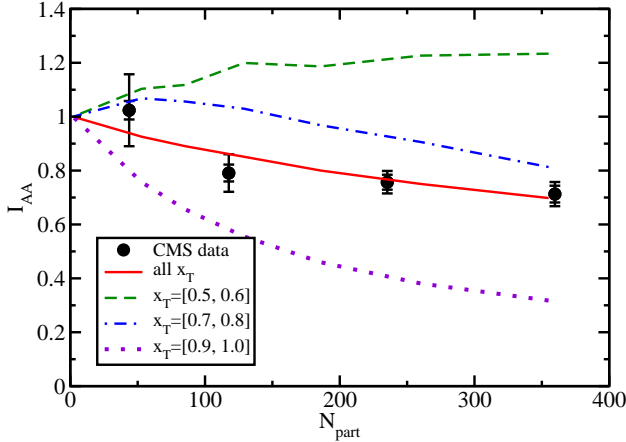

FIG. 9: (Color online) The nuclear modification factor I_{AA} for photon-triggered jets as a function of centrality for Pb+Pb collisions at the LHC. Results for different x_T values are compared. The jet size is $R = 0.3$.

Since the tagged jets with different final x_T values are mainly from different regions of QGP and traverse different lengths of the medium, they show different sensitivity to parton energy loss. In Fig. 9, we show nuclear modification factor I_{AA} for the photon-triggered jets as a function of centrality (N_{part}) for Pb+Pb collisions at the LHC. Results for different values of x_T bins are shown for comparison. The jet size is taken as $R = 0.3$ in this plot. Due to the combinational effects of different traveling distances and the tagged jet spectra, one observes different centrality dependence for the modification of photon-triggered jets with different values of x_T. Jets with larger values of x_T show larger suppression and stronger centrality dependence, while smaller suppression (or enhancement) is observed for smaller x_T jets.

III. SUMMARY

In this work, we have studied the medium modification of jets correlated with high p_T photons in Pb+Pb collisions at the LHC. A Monte-Carlo code is developed for simulating jet shower transport and modification in hot and dense QCD medium with the inclusion of both induced gluon radiation and the elastic collisions with the medium constituents. The effect of elastic collisions

experienced by the jet shower partons is encoded by a few non-perturbative transport coefficients such as the drag and diffusion, while the radiative energy loss is simulated by employing the single gluon emission spectrum from Higher Twist jet energy loss formalism.

With our event-by-event jet shower evolution code, we have presented the numerical results for the nuclear modification of photon-triggered jet production yield, the photon-jet momentum imbalance and their azimuth separation distribution. We have addressed the potential of photon-jet correlations as a tomographic tool for studying jet quenching in heavy-ion collisions by classifying photon-tagged jets with different values of the momentum fraction x_T. We found that jets with larger x_T values are mainly produced from the surface of the medium, while jets with smaller x_T values jets are mainly from these jets which have traversed longer distance. This makes photon-triggered jets very useful tomographic tools for studying jet modification in dense matter created in relativistic nuclear collisions. Combined with the tagged jet momentum spectrum, we found different sensitivity to parton energy loss for different photon-tagged jets: one observes stronger suppression and centrality dependence for larger x_T jets, and weaker suppression (or enhancement) for smaller x_T jets.

The above analysis may be directly applied for studying the nuclear modification of high p_T dijets and single inclusive jets. The inclusion of the hadronization process the for final partonic jet showers will enable us to directly compare to the experimental measurements of jet fragment profiles. The exploration of the sensitivity of jet modification to the properties of jet transport coefficients will help understand the detailed structure and properties of the dense QGP medium. The energy and momentum deposition profiles obtained from the simulation of in-medium jet shower evolution may be combined with hydrodynamics simulation to investigate the response of the medium to jet transport and the influence of hydrodynamic background and its fluctuations on full jet observables. These will be left in the follow-up effort.

Acknowledgments

[1] A. Majumder and M. Van Leeuwen, Prog.Part.Nucl.Phys. **A66**, 41 (2011), arXiv:1002.2206.

[2] PHENIX, K. Adcox *et al.*, Phys. Rev. Lett. **88**, 022301

(2002), arXiv:nucl-ex/0109003.

[3] STAR, C. Adler *et al.*, Phys. Rev. Lett. **89**, 202301 (2002), arXiv:nucl-ex/0206011.

[4] ALICE Collaboration, K. Aamodt *et al.*, Phys.Lett. **B696**, 30 (2011), arXiv:1012.1004.

[5] J. D. Bjorken, FERMILAB-PUB-82-059-THY.

[6] E. Braaten and M. H. Thoma, Phys.Rev. **D44**, 2625 (1991).

[7] B. Zakharov, JETP Lett. **63**, 952 (1996), arXiv:hep-ph/9607440.

[8] R. Baier, Y. L. Dokshitzer, A. H. Mueller, S. Peigne, and D. Schiff, Nucl. Phys. **B483**, 291 (1997), arXiv:hep-ph/9607355.

[9] G.-Y. Qin and A. Majumder, (2012), arXiv:1205.5741.

[10] M. Gyulassy, P. Levai, and I. Vitev, Nucl.Phys. **B571**, 197 (2000), arXiv:hep-ph/9907461.

[11] U. A. Wiedemann, Nucl.Phys. **B588**, 303 (2000), arXiv:hep-ph/0005129.

[12] P. B. Arnold, G. D. Moore, and L. G. Yaffe, JHEP **0111**, 057 (2001), arXiv:hep-ph/0109064.

[13] X.-N. Wang and X.-f. Guo, Nucl.Phys. **A696**, 788 (2001), arXiv:hep-ph/0102230.

[14] A. Majumder, Phys.Rev. **D85**, 014023 (2012), arXiv:0912.2987.

[15] N. Armesto *et al.*, (2011), arXiv:1106.1106.

[16] S. A. Bass *et al.*, Phys. Rev. **C79**, 024901 (2009), arXiv:0808.0908.

[17] S. Wicks, W. Horowitz, M. Djordjevic, and M. Gyulassy, Nucl. Phys. **A784**, 426 (2007), arXiv:nucl-th/0512076.

[18] G.-Y. Qin *et al.*, Phys. Rev. Lett. **100**, 072301 (2008), arXiv:0710.0605.

[19] N. Armesto, M. Cacciari, T. Hirano, J. L. Nagle, and C. A. Salgado, J. Phys. **G37**, 025104 (2010), arXiv:0907.0667.

[20] X.-F. Chen, C. Greiner, E. Wang, X.-N. Wang, and Z. Xu, Phys. Rev. **C81**, 064908 (2010), arXiv:1002.1165.

[21] H. Zhang, J. F. Owens, E. Wang, and X.-N. Wang, Phys. Rev. Lett. **98**, 212301 (2007), arXiv:nucl-th/0701045.

[22] T. Renk, Phys. Rev. **C78**, 034904 (2008), arXiv:0803.0218.

[23] T. Renk, Phys.Rev. **C74**, 034906 (2006), arXiv:hep-ph/0607166.

[24] G.-Y. Qin, J. Ruppert, C. Gale, S. Jeon, and G. D. Moore, Phys. Rev. **C80**, 054909 (2009), arXiv:0906.3280.

[25] H. Zhang, J. F. Owens, E. Wang, and X.-N. Wang, (2009), arXiv:0902.4000.

[26] I. Vitev and B.-W. Zhang, Phys. Rev. Lett. **104**, 132001 (2010), arXiv:0910.1090.

[27] N. Armesto, L. Cunqueiro, and C. A. Salgado, Eur. Phys. J. **C63**, 679 (2009), arXiv:0907.1014.

[28] K. Zapp, J. Stachel, and U. A. Wiedemann, PoS **HIGH-PTPHYSICS09**, 022 (2009), arXiv:0904.4885.

[29] B. Schenke, C. Gale, and S. Jeon, Phys. Rev. **C80**, 054913 (2009), arXiv:0909.2037.

[30] T. Renk, Int.J.Mod.Phys. **E20**, 1594 (2011), arXiv:1009.3740.

[31] G. Y. Qin, A. Majumder, H. Song, and U. Heinz, Phys. Rev. Lett. **103**, 152303 (2009), arXiv:0903.2255.

[32] R. B. Neufeld and B. Muller, Phys. Rev. Lett. **103**, 042301 (2009), arXiv:0902.2950.

[33] H. Li, F. Liu, G.-l. Ma, X.-N. Wang, and Y. Zhu, Phys.Rev.Lett. **106**, 012301 (2011), arXiv:1006.2893.

[34] Atlas Collaboration, G. Aad *et al.*, Phys.Rev.Lett. **105**, 252303 (2010), arXiv:1011.6182.

[35] CMS Collaboration, S. Chatrchyan *et al.*, Phys.Rev. **C84**, 024906 (2011), arXiv:1102.1957.

[36] J. Casalderrey-Solana, J. G. Milhano, and U. A. Wiedemann, J.Phys.G **G38**, 035006 (2011), arXiv:1012.0745.

[37] G.-Y. Qin and B. Muller, Phys.Rev.Lett. **106**, 162302 (2011), arXiv:1012.5280.

[38] I. Lokhtin, A. Belyaev, and A. Snigirev, Eur.Phys.J. **C71**, 1650 (2011), arXiv:1103.1853.

[39] C. Young, B. Schenke, S. Jeon, and C. Gale, Phys.Rev. **C84**, 024907 (2011), arXiv:1103.5769.

[40] Y. He, I. Vitev, and B.-W. Zhang, Phys.Lett. **B713**, 224 (2012), arXiv:1105.2566.

[41] C. Coleman-Smith, G.-Y. Qin, S. Bass, and B. Muller, AIP Conf.Proc. **1441**, 892 (2012), arXiv:1108.5662.

[42] T. Renk, Phys.Rev. **C85**, 064908 (2012), arXiv:1202.4579.

[43] X.-N. Wang, Z. Huang, and I. Sarcevic, Phys.Rev.Lett. **77**, 231 (1996), arXiv:hep-ph/9605213.

[44] PHENIX, A. Adare *et al.*, Phys. Rev. **C80**, 024908 (2009), arXiv:0903.3399.

[45] STAR, B. I. Abelev *et al.*, Phys. Rev. **C82**, 034909 (2010), arXiv:0912.1871.

[46] CMS Collaboration, S. Chatrchyan *et al.*, (2012), arXiv:1205.0206.

[47] R. Neufeld and I. Vitev, Phys.Rev.Lett. **108**, 242001 (2012), arXiv:1202.5556.

[48] W. Dai, I. Vitev, and B.-W. Zhang, (2012), arXiv:1207.5177.

[49] T. Sjostrand, S. Mrenna, and P. Z. Skands, Comput.Phys.Commun. **178**, 852 (2008), arXiv:0710.3820.

[50] M. Cacciari, G. P. Salam, and G. Soyez, Eur.Phys.J. **C72**, 1896 (2012), arXiv:1111.6097.

[51] H. Song and U. W. Heinz, Phys.Lett. **B658**, 279 (2008), arXiv:0709.0742.

[52] H. Song and U. W. Heinz, Phys.Rev. **C77**, 064901 (2008), arXiv:0712.3715.

[53] Z. Qiu, C. Shen, and U. Heinz, Phys.Lett. **B707**, 151 (2012), arXiv:1110.3033.

[54] A. Majumder, (2012), arXiv:1202.5295.